A New Series of Mixed-Valence Titanium(III/IV) Phosphates, $Li_{1+x}Ti_2(PO_4)_3$ ($0 \le x \le 2$), with NASICON-Related Structures

Shumin Wang and Shiou-Jyh Hwu*

Department of Chemistry, Rice University, P.O. Box 1892, Houston, Texas 77251

Received October 8, 1991. Revised Manuscript Received January 21, 1992

A new series of nonstoichiometric lithium titanium(III/IV) phosphates, $Li_{1+x}Ti_2(PO_4)_3$ ($0 \le x \le 2$), has been systematically studied. The structure of a relatively low lithium composition phase ($x = 0.78$) has been characterized by single-crystal X-ray diffraction. This newly synthesized $Li_{1.78}Ti_2(PO_4)_3$ phase crystallizes in the orthorhombic system, *Pbca* (No. 61), with $a = 8.667$ (3) Å, $b = 23.968$ (6) Å, $c = 8.565$ (2) Å, $V = 1779.2$ (9) Å^3, and $Z = 8$. This compound, essentially a mixed-valence titanium(III/IV) phosphate, presents an original structure which is related to that of NASICON. The structure comparison with the previously reported $x = 1.72$ phase (*J. Solid State Chem.* **1991**, *90*, 377) as well as the $x = 0.00$ phase (NASICON structure) and the phase relationship to the known $Li_{1+x}Ti_{2-x}^{IV}In_x^{III}(PO_4)_3$ series are discussed. Studies of open framework structures and mixed valency in the $Li_{1+x}Ti_{2-x}^{IV}Ti_x^{III}(PO_4)_3$ solid solution series have suggested some interesting features that are presumably of importance to fast ionic conductivity.

Introduction

Interest in the areas of ion exchangers[1] and solid electrolytes[2] has stimulated research into frameworks with sizable channels.[3] Since the discovery of fast Na^+ ion transport in NASICON (the acronym for Na superionic conductor), $Na_{1+x}Zr_2Si_xP_{3-x}O_{12}$,[4] its structurally related compounds have been extensively studied. In the NASICON series, compositions with $1.8 < x < 2.3$ exhibit the highest conductivities and are competitive with the best β- and β''-alumina.[5] Structural studies of NASICON-related phosphate compounds with the general formula $A_xM_2(PO_4)_3$ have shown that the frameworks are characterized by $M_2(PO_4)_3$ units (1). Each unit consists of two

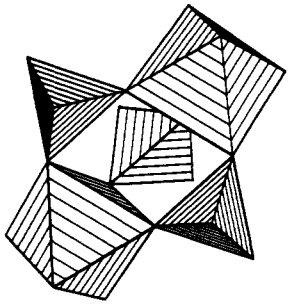

(1)

MO_6 octahedra that are connected through corner-sharing PO_4 tetrahedra. The A-site cation, which is the mobile cation, has demonstrated its role in determining the structure type and, moreover, the size of the openings for ion diffusion.

Compounds forming NASICON or related structures constitute a very large class of solid-state compounds. Transition-metal and post-transition-metal cations with tri- or tetravalent oxidation states can almost always be found to substitute for zirconium in NASICON. The concentration of the electropositive A-site cation varies to counterbalance the charge for isoelectronic substitution and/or solid solution formation. An example of this is shown in the indium-substituted lithium titanium phosphate solid solution series, $Li_{1+x}Ti_{2-x}^{IV}In_x^{III}(PO_4)_3$.[6] The best conductivity measured for this series, 2×10^{-2} $(\Omega\ cm)^{-1}$ for $x \approx 0.35$, at 300 °C,[7] is a factor of 10 lower than that of NASICON.

Studies of the NASICON-related phosphate compounds have shown that $LiTi_2(PO_4)_3$ is a much better Li^+ conductor than $LiZr_2(PO_4)_3$.[8] This might be attributed to the weaker Li–O interactions in the titanium compound than those in the zirconium analogue because of the stronger O 2p–Ti 3d orbital overlap in comparison with the weaker O 2p–Zr 4d overlap. Therefore, we have continued the study of the synthesis and structure of the reduced lithium titanium phosphate solid solution series, $Li_{1+x}Ti_{2-x}^{IV}Ti_x^{III}(PO_4)_3$, where the smaller trivalent titanium cation (Ti^{3+}) has been substituted for indium (In^{3+}).

A new compound with an original structure has been discovered at the lower end of the lithium concentration, e.g., $Li_{1+x}Ti_2(PO_4)_3$ ($x = 0.78$). In this paper, the structure comparisons to the $x = 0.00$ and 1.72[9] phases are described. Detailed phase analysis for the newly synthesized solid solution series is also presented.

Experimental Section

Synthesis. Single crystals of the new titanium(III/IV) phosphate compound, $Li_{1+x}Ti_2(PO_4)_3$ ($x = 0.78$), were obtained from the reduced system, Li_2O–TiO_z–P_2O_5 ($z < 2$). The reaction conditions and experimental procedures were the same as previously described.[9] It is known that controlling the lithium compositions in the synthesis is difficult. By using a low-temperature, solid-state precursor method and a sealed reaction container (to prevent the oxidation of reduced components and the loss of Li_2O), sizable single crystals with the desired x value can be isolated. The molar ratios for obtianing the $x = 0.78$ phase

* To whom all correspondence should be addressed.

(1) Clearfield, A. *Chem. Rev.* **1988**, *88*, 125.
(2) (a) Vashishta, P.; Mundy, J. N.; Shenoy, G. K. In *Fast Ion Transport in Solids Electrodes and Electrolytes*; North-Holland, Inc: Amsterdam, 1979. (b) Laskar, A. L.; Chandra, S. In *Superionic Solids and Solid Electrolytes Recent Trends*; Academic Press, Inc.: New York, 1989.
(3) Wang, E.; Greenblatt, M. *Chem. Mater.* **1991**, *3*, 542 and references therein.
(4) (a) Hong, H. Y.-P. *Mater. Res. Bull.* **1976**, *11*, 173. (b) Goodenough, J. B.; Hong, H. Y.-P.; Kafalas, J. A. *Mater. Res. Bull.* **1976**, *11*, 203.
(5) (a) Yao, Y.-F. Y.; Kummer, J. T. *J. Inorg. Nuclear Chem.* **1967**, *29*, 2453. (b) Whittingham, M. S. *J. Chem. Phys.* **1971**, *54*, 414. (c) Briant, J. L.; Farrington, G. C. *J. Solid State Chem.* **1980**, *33*, 385.
(6) (a) Li, S.-C.; Lin, Z.-X. *Solid State Ionics* **1983**, *10*, 835. (b) Tran Qui, D.; Hamdoune, S.; Soubeyroux, J. L.; Prince, E. *J. Solid State Chem.* **1988**, *72*, 309.
(7) (a) Hamdoune, S.; Tran Qui, D.; Schouler, E. J. L. *Solid State Ionics* **1986**, *18/19*, 587. (b) Tran Qui, D.; Hamdoune, S. *Acta Crystallogr.* **1987**, *C43*, 397.
(8) (a) Lin, Z.-X.; Yu, H.-J.; Li, S.-C.; Tian, S.-B. *Solid State Ionics* **1986**, *18/19*, 549. (b) Subramanian, M. A.; Subramanian, R.; Clearfield, A. *Solid State Ionics* **1986**, *18/19*, 562.
(9) Wang, S.; Hwu, S.-J. *J. Solid State Chem.* **1991**, *90*, 377.

0897-4756/92/2804-0589$03.00/0

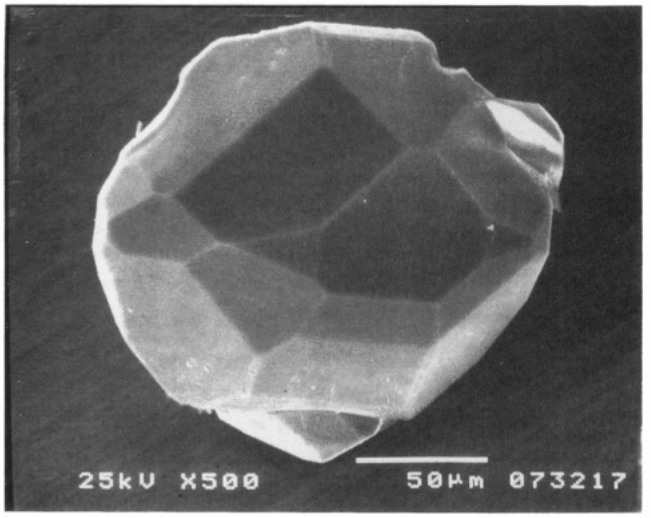

Figure 1. Scanning electron micrography of a gem crystal of $Li_{1+x}Ti_2(PO_4)_3$.

are $Li_2O:TiO_z:P_2O_5$ = 0.8:2.0:1.5 (z = 1.85).

Under a scanning electron microscope (SEM), the morphology of the $Li_{1+x}Ti_2(PO_4)_3$ single crystals revealed a multifaceted geometry, as shown in Figure 1. The average size of the crystals ranged from 0.10 to 0.35 mm in diameter. The single-crystalline material had very attractive, black shiny surfaces and retained the same appearance for long periods of time in air.

High purity, polycrystalline samples of the series $Li_{1+x}Ti_2(PO_4)_3$ ($0 \le x \le 2$) were synthesized by stoichiometric reactions using the same procedures as mentioned above. For samples with $x \le 1.20$, a certain amount of a second phase, identified by XRD patterns as $LiTiP_2O_7$,[10] was detected in the reaction mixture after the first heating. Thus intermittent grindings were needed to prepare high purity (ca. 95%) polycrystalline materials. With increasing lithium composition (x), the color of the reaction product changed from light blue ($0.00 < x \le 0.50$) to bluish black ($0.50 < x \le 2.00$).

X-ray Structure Analysis. *Single-Crystal Structure Determination.* A gem crystal was mounted on the tip of a glass fiber with epoxy cement for single-crystal X-ray structure examination. The initial unit-cell parameters and orientation matrix were derived from the least-squares fit of 25 reflections ($6° \le 2\theta \le 16°$) for data collection. The Laue patterns showed a primitive orthorhombic crystal system (*mmm*), which is consistent with the symmetry observed in Weissenberg photographs. Data were collected using a Rigaku AFC5S automated four-circle diffractometer through the range $0 \le h \le 11$, $-31 \le k \le 31$, $0 \le l \le 11$. The detailed crystallographic data are listed in Table I. Three standards (2, −2, 1; 0, −6, −1; 2, −3, 1), which were measured every 150 reflections, showed essentially no measurable decay in intensity. The TEXSAN[11] software package was used for crystal structure solution and refinement. Data reduction, intensity analysis, and space group determination were accomplished with the program PROCESS. On the basis of the intensity statistics, systematic extinctions (observed $0kl$: $k = 2n$; $h0l$: $l = 2n$; $hk0$: $h = 2n$), and the successful structure refinement, the space group was determined to be *Pbca* (No. 61). Three azimuthal scans (2θ = 10.75°, 11.15°, 13.38°) were used for absorption corrections. The atomic coordinates of the heavier cations (Ti and P) were found by SHELXS-86.[12] The positional parameters of the 12 oxygen atom sites and two fully occupied lithium sites, Li(1) and Li(2), were then located from the Fourier difference maps. The structural and thermal parameters were refined by full-matrix least-squares methods based on F^2 to R = 0.036, R_w = 0.051, and GOF = 1.81. This led to a structural composition of $Li_{1.50}Ti_2(PO_4)_3$.

Table I. Crystallographic Data for $Li_{1.78}Ti_2(PO_4)_3$

formula mass (amu)	393.07
space group	*Pbca* (No. 61)
cell parameters[a]	
a, Å	8.667 (3)
b, Å	23.968 (6)
c, Å	8.565 (2)
V, Å^3	1779.2 (9)
Z	8
T of data collection, K	296
ρ_{calc}, g cm^{-3}	2.93
radiation (graphite monochromated)	Mo Kα (λ = 0.71069 Å)
crystal shape, color	gem, bluish black
crystal size, mm	0.25 × 0.20 × 0.12
linear abs coeff, cm^{-1}	23.75
transmission factors	0.94–1.00
scan type	ω scan
scan speed, deg min^{-1}	4.0
scan range, deg	−0.45° to 0.45° in ω
background counts	$^1/_4$ of scan range on each side of reflection
2θ(max), deg	55
data collected	$h,\pm k,l$
p for $\sigma(F^2)$	0.03
no. of unique data ($F_o^2 > 0$)	2036
no. of unique data with $F_o^2 > 3\sigma(F_o^2)$	1560
F_{000}	1522.72
$R(F^2)$[b]	0.037
$R_w(F^2)$[b]	0.050
R_{int} (on F for $F_o^2 > 3\sigma(F_o^2)$)	0.025
goodness of fit	1.79
no. of variables	177

[a] The refinement of cell constants is constrained in the orthorhombic crystal system, using the first 25 strongest reflections in $35° \le 2\theta \le 45°$. [b] $R = \sum[|F_o| - |F_c|]/\sum|F_o|$; $R_w = [\sum w[|F_o| - |F_c|]^2/\sum w|F_o|^2]^{1/2}$.

The positions of two additional lithium sites, Li(3) and Li(4), were first derived from the $Li_{2.72}Ti_2(PO_4)_3$ structure, which contains partially occupied lithium sites in similar channels. The estimated positions were (0.25, 0.02, 0.33) and (0.30, 0.23, 0.16) for Li(3) and Li(4), which were then refined to the new positions (0.26, 0.05, 0.34) and (0.29, 0.20, 0.13), respectively. The occupancy factors were also refined and showed partial occupancies with similar values, e.g., 0.15 (3) for Li(3) and 0.13 (3) for Li(4). Subsequently, the least-squares refinement converged and resulted in a new set of values; R = 0.037, R_w = 0.050, and improved GOF = 1.79 for a final structural composition of $Li_{1.78}Ti_2(PO_4)_3$.

It should be noted that alternate lithium positions, such as the center of nonoccupied channels, have been refined with the same level of partial occupancy; however, refinement of the positional parameters diverged. This indicated that the refined values are substantial for the two nonstoichiometric lithium sites Li(3) and Li(4), although the changes in R values are minimal, as expected. The final positional and thermal parameters are given in Table II.

Powder X-ray Diffraction. Powder X-ray diffraction (XRD) patterns of the polycrystalline samples were recorded at room temperature on a Philips PW 1840 Diffractometer (with Cu Kα radiation, λ = 1.5418 Å, and a Ni filter). The experimental procedures were the same as previously described.[13] The XRD patterns ($5° \le 2\theta \le 60°$) were indexed and the cell constants were refined by the program POLSQ.[14] The refinements were constrained in a designated crystal system (orthorhombic or hexagonal) and included 14–28 reflections. In Table III, the refined cell constants of the three structurally characterized phases are listed.

Thermal Analysis. Thermal analysis (by Du Pont 9900 Thermal Analysis System) was performed for the entire solid solution series using thermogravimetric analysis (TGA) and differential thermal analysis (DTA) methods. TGA experiments

(10) Wang, S.; Hwu, S.-J. *J. Solid State Chem.* **1991**, *92*, 219.
(11) TEXSAN: Single Crystal Structure Analysis Software, Version 5.0; Molecular Structure Corp.: The Woodlands, TX, 1989.
(12) Sheldrick, G. M. In *Crystallographic Computing 3*; Sheldrick, G. M., Krüger, C.; Goddard, R., Eds.; Oxford University Press: London, pp 175–189, 1985.
(13) Wang, S.; Hwu, S.-J. *J. Solid State Chem.* **1991**, *90*, 31.
(14) Keszler, D.; Ibers, J. POLSQ, FORTRAN program, Northwestern University, 1983.
(15) PDF, No. 35–754, JCPDS-International Center for Diffraction Data, Swarthmore, PA.

Table II. Positional and Isothermal Temperature Parameters for $Li_{1.78}Ti_2(PO_4)_3$

atom	x	y	z	B_{eq},[a] Å^2
Ti(1)	0.2154 (1)	0.43153 (3)	0.4996 (1)	0.49 (3)
Ti(2)	0.2885 (1)	0.17892 (3)	0.4966 (1)	0.53 (3)
P(1)	0.3674 (1)	0.44738 (5)	0.1533 (1)	0.54 (4)
P(2)	0.1496 (1)	0.30090 (5)	0.3576 (1)	0.48 (4)
P(3)	0.4995 (1)	0.12090 (5)	0.2100 (1)	0.53 (4)
O(1)	0.2632 (4)	0.4899 (1)	0.0710 (4)	1.0 (1)
O(2)	0.0381 (4)	0.4568 (1)	0.3872 (4)	1.0 (1)
O(3)	0.3546 (4)	0.4558 (1)	0.3303 (4)	0.8 (1)
O(4)	0.3190 (4)	0.3890 (1)	0.1058 (4)	1.2 (1)
O(5)	0.2054 (4)	0.3580 (1)	0.4169 (4)	1.1 (1)
O(6)	0.2662 (3)	0.2582 (1)	0.4191 (4)	0.9 (1)
O(7)	0.4889 (4)	0.2872 (1)	0.0799 (4)	0.9 (1)
O(8)	0.1461 (4)	0.2990 (1)	0.1800 (4)	0.9 (1)
O(9)	0.4128 (4)	0.0776 (1)	0.1121 (4)	1.0 (1)
O(10)	0.1104 (4)	0.0885 (1)	0.1852 (4)	1.2 (1)
O(11)	0.0847 (4)	0.1604 (1)	0.4011 (4)	1.1 (1)
O(12)	0.3884 (4)	0.1557 (2)	0.3058 (4)	1.6 (2)
Li(1)	0.470 (1)	0.2861 (4)	0.464 (1)	1.6 (4)
Li(2)	0	0	1/2	5 (1)
Li(3)[b]	0.26 (1)	0.050 (4)	0.34 (1)	4[c]
Li(4)[b]	0.29 (1)	0.197 (5)	0.13 (1)	4[c]

[a] Anisotropically refined atoms are given in the form of the isotropic equivalent displacement parameters defined as $B_{eq} = (8\pi^2/3)$ trace U. [b] Refined occupancy factors for Li(3) and Li(4) are 0.15 (3) and 0.13 (3), respectively. [c] The B_{eq} parameters (Å^2) were initially refined, resulting in values of 11 (2) and 10 (3) and occupancy factors of 0.26 (6) and 0.22 (5) for Li (3) and Li (4), respectively. Ultimately, the fixed isotropic thermal parameters were obtained from the B_{eq} for Li (2) in the $x = 1.72$ phase.[9] This alternation does not effect the R/GOF values but more importantly is consistent with the results from the studies of polycrystalline samples.

Table III. Refined Lattice Parameters[a] for Polycrystalline $Li_{1+x}Ti_2(PO_4)_3$ (x = 0.00, 0.78, and 1.72)

	$LiTi_2(PO_4)_3$[b]	$Li_{1.78}Ti_2(PO_4)_3$	$Li_{2.72}Ti_2(PO_4)_3$
space group	$R\bar{3}c$	*Pbca*	*Pbcn*
a, Å	8.520 (2)	8.657 (5)	12.072 (5)
b, Å	=*a*	24.02 (1)	8.664 (4)
c, Å	20.87 (1)	8.550 (6)	8.724 (4)
V, Å^3	1312.1 (8)	1778 (2)	912.5 (7)
no. of reflections[c]	20	28	23

[a] The refinement of cell constants is constrained to the designated crystal system. [b] For comparison, the reported cell constants are a = 8.5129 (8) Å, c = 20.87 (4) Å.[15] [c] $I_{obs} \geq 5$ and $I_{max} = 100$.

were carried out according to procedures used previously.[13] The analyses (25–900 °C) of polycrystalline samples (ca. 20 mg) showed a weight gain corresponding to the oxidative decomposition of $Ti^{3+} \rightarrow Ti^{4+}$. The starting decomposition point for the title series generally occurred at approximately 550 °C.

Phase transformation is a commonly seen phenomenon in NASICON and related compounds and has a close relationship with the transport properties.[16] An upper temperature limit of T_{max} = 300 °C was chosen for the DTA analyses in an open system with flowing nitrogen. (A platinum crucible was used to contain the polycrystalline sample, ca. 25 mg/run.) Complicated reversible phase transitions were observed in the high lithium concentration region of the solid solution series, i.e., $1.20 \leq x \leq 2.00$. It is important to note that, under the above stated DTA experimental conditions, samples survived repeated heating cycles (according to XRD and oxidative decomposition TGA analyses). The detailed phase transformation and ionic conductivity relationship will be reported at a later date.

Results and Discussion

Solid Solution Series, $Li_{1+x}Ti_2(PO_4)_3$. The phase relationship of the entire series is demonstrated by the normalized volume (per four formula units) vs lithium composition (x) curve, as shown in Figure 2. The dotted line is drawn to show the trend in cell volume. At first glance, there are three regions of the curve that follow Vegard's law. These regions alternate with three plateaus where phase separation may exist. A close examination of the XRD patterns of the compound series shows that the solid solution limits are found to be surprisingly different than expected, e.g., $0.00 \leq x \leq 0.50$ (I), $0.50 < x < 1.20$ (II) and $1.20 \leq x \leq 2.00$ (III). These three regions represent the extended solid solutions of the x = 0.00, 0.78, and 1.72 phases (Table III), respectively. The constant volumes in the plateau regions may be attributed to some possible lattice rearrangement which results in a cell volume contraction. This phenomenon compensates for the expected cell expansion due to the reduction of $Ti^{4+} \rightarrow Ti^{3+}$. A possible lattice rearrangement could be attributed to the flexible channel structures. This flexibility is also seen in the NASICON structure where, for example, a structural transformation occurs from $R\bar{3}c$ to $C2/c$[17] due to a rotation of the tetrahedral groups. An orthorhombic to monoclinic structural distortion may occur in our system. However, the change is too small to be distinguished by the powder X-ray diffraction method.

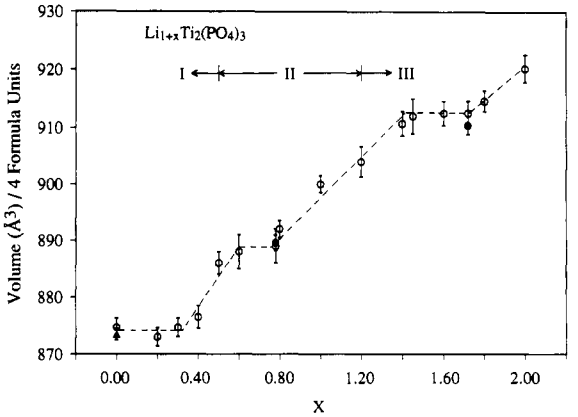

Figure 2. Normalized cell volume (3σ limits) vs x plot for $Li_{1+x}Ti_2(PO_4)_3$, $0.00 \leq x \leq 2.00$. The dotted line is drawn to demonstrate the trend in changing cell volume. The three solid solution regions are $0.00 \leq x \leq 0.50$ (I), $0.50 < x < 1.20$ (II), and $1.20 \leq x \leq 2.00$ (III). The cell volumes for the $x = 0.00$ (ref 15, solid triangle), 0.78, and 1.72 (single-crystal data, solid circles) phases are also included for comparison.

In region I, further structural studies are needed. The XRD patterns of the lower end of this solid solution series were mostly indexed according to the $LiTi_2(PO_4)_3$ phase. Some reflections, with relative intensity less than 10, are not matchable with any of the known phases, including the pseudo-binary titanium phosphate. The three strongest reflections that are unindexed have d spacings of 2.167, 2.519, and 2.823 Å. We speculate that a third phase may exist with a structure slightly distorted from that of the fully oxidized phase ($x = 0.0$).

It should be noted that the volume vs x curve for the $Li_{1+x}Ti_{2-x}^{IV}In_x^{III}(PO_4)_3$ phase[7] breaks down in a fashion similar to that observed in the title system. That is to say, the volume discontinuity caused by phase separation occurs at approximately the same regions (between the plateaus) presented above. This phenomena, which is not seen in the NASICON series, is presumably attributed to the separation of the tetravalent and trivalent sites, Ti^{4+}/Ti^{3+} in the current system (see later discussion). The two separated asymmetric titanium sites are ordered and subsequently give rise to a superlattice which causes the

(16) (a) Sudreau, F.; Petit, D.; Boilot, J. P. *J. Solid State Chem.* **1989**, *83*, 78. (b) d'Yvoire, F.; Pintard-Scrépel, M.; Bretey, E.; de la Rochère, M. *Solid State Ionics* **1983**, *9*, 851.

(17) Boilot, J. P.; Salanié, J. P.; Desplanches, G.; Le Potier, D. *Mater. Res. Bull.* **1979**, *14*, 1469.

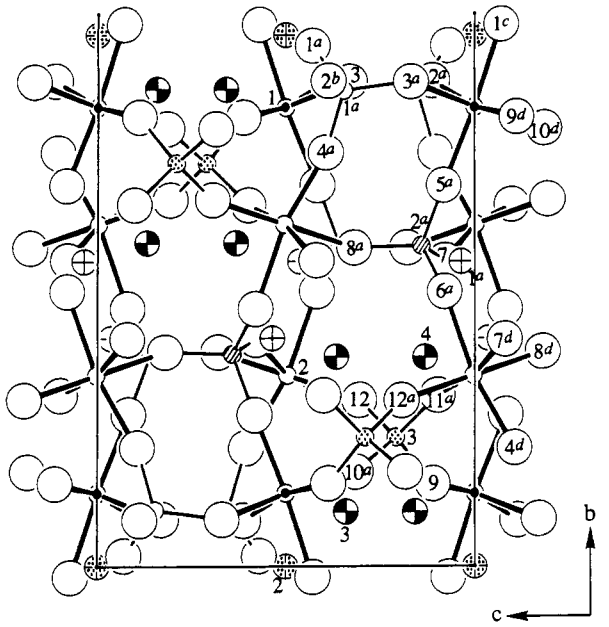

Figure 3. ORTEP drawing of half a unit cell of the projected structure of $Li_{1.78}Ti_2(PO_4)_3$ viewed along the a axis. The octahedrally coordinated Ti-O bonds are drawn in heavy lines. The small circles are titanium and phosphorus; Ti(1) (singly dotted), Ti(2) (open), P(1) (open), P(2) (shaded), P(3) (multiple dotted). The inside numbered large open circles are oxygens. The cross-hatched medium circles are lithium atoms. The half-filled circles (along a different diagonal) are partially occupied Li sites, Li(3) and Li(4) (see text). Symmetry codes: $a = {}^1/_2 + x, y, {}^1/_2 - z$; $b = 1 + x, y, z$; $c = 1 - x, 1 - y, -z$; $d = {}^1/_2 + x, {}^1/_2 - y, -z$.

doubling of the longest unit cell axis, b, compared to that in the $x = 1.72$ phase (Table III).

Single-Crystal Structure of $Li_{1+x}Ti_2(PO_4)_3$, $x = 0.78$. In Figure 3, half of the unit cell ($Z/2 = 4$) of $Li_{1.78}Ti_2(PO_4)_3$ is viewed along the a axis. The second half of the unit cell is generated by an inversion center occurring at $({}^1/_2, {}^1/_2, {}^1/_2)$. This structure contains isolated TiO_6 octahedra (drawn in thick lines) which share each of their six corner oxygen atoms with a PO_4 tetrahedron. In the network, each asymmetric unit consists of two titanium atoms, three phosphorus atoms, and twelve oxygen atoms. In addition, there are four lithium atoms per asymmetric unit, two of which are in the cages, Li(1) and Li(2), and two of which are in the channels, Li(3) and Li(4). The Li(3) and Li(4) sites are partially occupied with refined occupancy factors of 0.15 and 0.13, respectively.

The atomic arrangement of the $x = 0.78$ compound is similar to that of the $x = 1.72$ phase in that both structures have $Ti_2(PO_4)_3$ frameworks which contain sizable channels with similar geometries. In both compounds there are two channel structures, one with a large pseudo-pentagonal window and one with a small octagonal window. Figure 4 shows a STRUPLO polyhedral representation of the projected unit cell framework of $Li_{1.78}Ti_2(PO_4)_3$, which is viewed along the channels. This framework is built up from corner sharing TiO_6 octahedra and PO_4 tetrahedra. The lithium atoms, omitted for clarity, reside in the pseudo-pentagonal channels (T1 and T2) and in the cages between the two parallel channels, which are next to each other along the c axis. In viewing Figures 3 and 4, one recognizes that the partially occupied Li(3) and Li(4) sites are in the T1 and T2 channels, respectively, which may facilitate pathways for conducting Li^+ ions. The pentagonal windows are characterized by minimum/maximum diagonal O–O distances of 4.54 Å/5.31 Å for T1 and 5.21 Å/6.23 Å for T2, which are significantly longer than 2 times the Li–O distance (2 × 2.16 Å = 4.32 Å) according to the

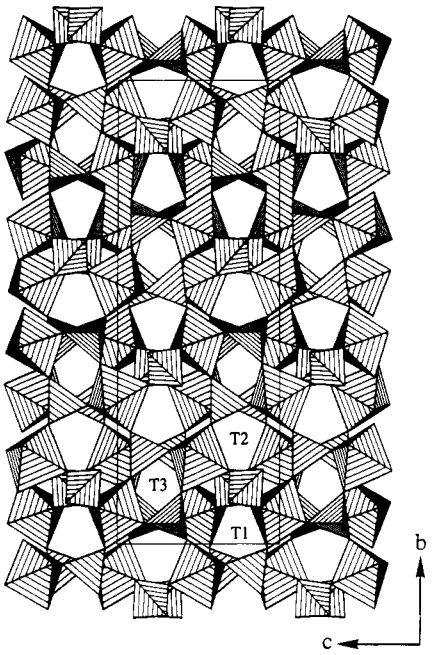

Figure 4. Projected STRUPLO 86 polyhedral representation of the structure of $Li_{1.78}Ti_2(PO_4)_3$ is viewed along a. The lithium atoms are omitted for clarity. The unit cell projected on the bc plane is outlined. The two parallel channels, T1 and T2, are partially occupied by Li(3) and Li(4), respectively, while T3 is empty.

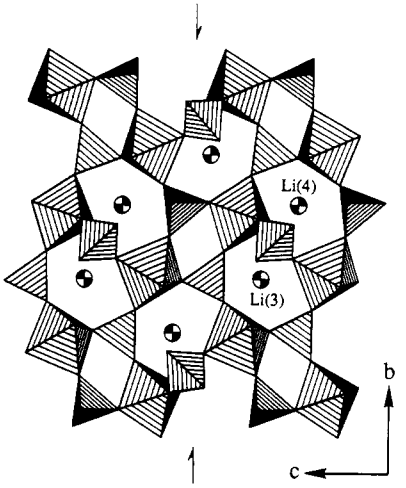

Figure 5. The partial structure of $Li_{1.78}Ti_2(PO_4)_3$ is shown by a single slab projected onto the bc plane. The arrows indicate the position of an a-glide symmetry plane.

six coordinated Shannon crystal radii.[18] The neighboring octagonal channels are evidently empty. This may be because the size of the vacant site is too small for a single lithium atom. The octagonal channels in the structure of the $x = 1.72$ phase are also empty.

In spite of the complexity of the structure, the framework can be viewed as corner-sharing TiO_6 and PO_4 octahedral slabs that are stacked along the a axis. Figure 5 shows a partial structure of the $Li_{1.78}Ti_2(PO_4)_3$ phase, where two types of voids are formed by various numbers of corner-sharing polyhedra. The larger void (centered by Li(3) or Li(4) atoms) is characterized by three TiO_6 octahedra and three PO_4 tetrahedra (3O and 3T) and is responsible for the formation of the pseudo-pentagonal channels (T1 or T2, respectively). These channels are formed by the stacking together of two slabs that are symmetry related by an a-glide plane, as indicated by the

(18) Shannon, R. D. *Acta Crystallogr.* **1976**, *A32*, 751.

Table IV. Important Bond Distances (Å) and Angles (deg) for $Li_{1.78}Ti_2(PO_4)_3$[a]

	TiO_6 Octahedra		
Ti(1)[e]–O(1)[f]	1.989 (3)	Ti(2)[e]–O(4)[g]	1.896 (3)
Ti(1)[e]–O(2)[e]	1.911 (3)	Ti(2)[e]–O(6)[e]	2.022 (3)
Ti(1)[e]–O(3)[e]	1.974 (3)	Ti(2)[e]–O(7)[g]	2.046 (3)
Ti(1)[e]–O(5)[e]	1.901 (3)	Ti(2)[e]–O(8)[g]	2.067 (3)
Ti(1)[e]–O(9)[g]	1.976 (3)	Ti(2)[e]–O(11)[e]	1.997 (4)
Ti(1)[e]–O(10)[g]	1.893 (3)	Ti(2)[e]–O(12)[e]	1.931 (4)
O(1)[f]–Ti(1)[e]–O(2)[e]	86.0 (1)	O(4)[g]–Ti(2)[e]–O(6)[e]	169.1 (2)
O(1)[f]–Ti(1)[e]–O(3)[e]	83.7 (1)	O(4)[g]–Ti(2)[e]–O(7)[g]	92.9 (1)
O(1)[f]–Ti(1)[e]–O(5)[e]	175.2 (2)	O(4)[g]–Ti(2)[e]–O(8)[g]	85.9 (1)
O(1)[f]–Ti(1)[e]–O(9)[g]	82.8 (1)	O(4)[g]–Ti(2)[e]–O(11)[e]	97.7 (1)
O(1)[f]–Ti(1)[e]–O(10)[g]	91.5 (2)	O(4)[g]–Ti(2)[e]–O(12)[e]	96.2 (2)
O(2)[e]–Ti(1)[e]–O(3)[e]	91.6 (1)	O(6)[e]–Ti(2)[e]–O(7)[g]	79.8 (1)
O(2)[e]–Ti(1)[e]–O(5)[e]	94.0 (1)	O(6)[e]–Ti(2)[e]–O(8)[g]	87.2 (1)
O(2)[e]–Ti(1)[e]–O(9)[g]	167.6 (1)	O(6)[e]–Ti(2)[e]–O(11)[e]	89.4 (1)
O(2)[e]–Ti(1)[e]–O(10)[g]	96.7 (2)	O(6)[e]–Ti(2)[e]–O(12)[e]	92.1 (2)
O(3)[e]–Ti(1)[e]–O(5)[e]	91.5 (1)	O(7)[g]–Ti(2)[e]–O(8)[g]	98.0 (1)
O(3)[e]–Ti(1)[e]–O(9)[g]	82.0 (1)	O(7)[g]–Ti(2)[e]–O(11)[e]	169.2 (1)
O(3)[e]–Ti(1)[e]–O(10)[g]	170.1 (1)	O(7)[g]–Ti(2)[e]–O(12)[e]	91.7 (2)
O(5)[e]–Ti(1)[e]–O(9)[g]	96.8 (1)	O(8)[g]–Ti(2)[e]–O(11)[e]	80.8 (1)
O(5)[e]–Ti(1)[e]–O(10)[g]	93.2 (2)	O(8)[g]–Ti(2)[e]–O(12)[e]	170.0 (2)
O(9)[g]–Ti(1)[e]–O(10)[g]	88.8 (1)	O(11)[e]–Ti(2)[e]–O(12)[e]	89.2 (1)
	PO_4 Tetrahedra		
P(1)[e]–O(1)[e]	1.533 (3)	P(2)[e]–O(7)[a]	1.528 (3)
P(1)[e]–O(2)[a]	1.536 (4)	P(2)[e]–O(8)[e]	1.522 (3)
P(1)[e]–O(3)[e]	1.534 (3)	P(3)[e]–O(9)[e]	1.532 (3)
P(1)[e]–O(4)[e]	1.516 (3)	P(3)[e]–O(10)[a]	1.528 (3)
P(2)[e]–O(5)[e]	1.538 (3)	P(3)[e]–O(11)[a]	1.531 (4)
P(2)[e]–O(6)[e]	1.531 (3)	P(3)[e]–O(12)[e]	1.515 (4)
O(1)[e]–P(1)[e]–O(2)[a]	111.5 (2)	O(6)[e]–P(2)[e]–O(7)[a]	109.7 (2)
O(1)[e]–P(1)[e]–O(3)[e]	108.9 (2)	O(6)[e]–P(2)[e]–O(8)[e]	109.7 (2)
O(1)[e]–P(1)[e]–O(4)[e]	109.1 (2)	O(7)[a]–P(2)[e]–O(8)[e]	109.0 (2)
O(2)[a]–P(1)[e]–O(3)[e]	105.9 (2)	O(9)[e]–P(3)[e]–O(10)[a]	106.6 (2)
O(2)[a]–P(1)[e]–O(4)[e]	109.9 (2)	O(9)[e]–P(3)[e]–O(11)[a]	108.4 (2)
O(3)[e]–P(1)[e]–O(4)[e]	111.5 (2)	O(9)[e]–P(3)[e]–O(12)[e]	111.0 (2)
O(5)[e]–P(2)[e]–O(6)[e]	105.9 (2)	O(10)[a]–P(3)[e]–O(11)[a]	112.1 (2)
O(5)[e]–P(2)[e]–O(7)[a]	111.3 (2)	O(10)[a]–P(3)[e]–O(12)[e]	111.2 (2)
O(5)[e]–P(2)[e]–O(8)[e]	111.3 (2)	O(11)[a]–P(3)[e]–O(12)[e]	107.6 (2)

[a] Symmetry codes: e = x, y, z; f = $^1/_2 - x, 1 - y, ^1/_2 + z$; g = $x, ^1/_2 - y, ^1/_2 + z$.

arrows in Figure 5. The smaller size void, corresponding to the octagonal channel (T3), is formed by two octahedra and two tetrahedra (2O and 2T). The same channel structure formation is found in the structures of the x = 0.00 (NASICON structure) and 1.72 phases.

Doubling of the longest axis in the structure of the x = 0.78 phase, compared with that of the x = 1.72, is attributed to the separation of Ti^{3+} and Ti^{4+} in the solid solution region II, i.e., $Li_{1+x}Ti_{2-x}^{IV}Ti_x^{III}(PO_4)_3$, $0.50 < x < 1.20$. A cation ordering is strongly indicated by the following observations in the X-ray single-crystal structure solution. The observed Ti–O bond distances (Table IV) span two ranges, 1.89–1.99 Å for Ti(1)–O and the little longer distances of 1.90–2.07 Å for Ti(2)–O. They are comparable with the sum of the Shannon crystal radii,[18] i.e., 2.01 Å for tetravalent Ti(IV)–O and 2.07 Å for trivalent Ti(III)–O, respectively. The bond valence sum calculations, using the observed Ti–O bond distances and the formula derived by Brown and Altermatt,[19] result in the valence values of 4.3 for Ti(1) and 3.8 for Ti(2). While these bond valence values may require some calibration, they suggest that the Ti(2) site is formally more reduced than the Ti(1) site. Furthermore, the bond distance range for the Ti(2)–O bonds is closely related to that fond in the x = 1.72 phase (1.92–2.08 Å), where the formal oxidation state of titanium cations is mostly 3+ (confirmed by magnetic susceptibility experiments[9]).

(19) Brown, I. D.; Altermatt, A. *Acta Crystallogr.* **1985**, *B41*, 244.

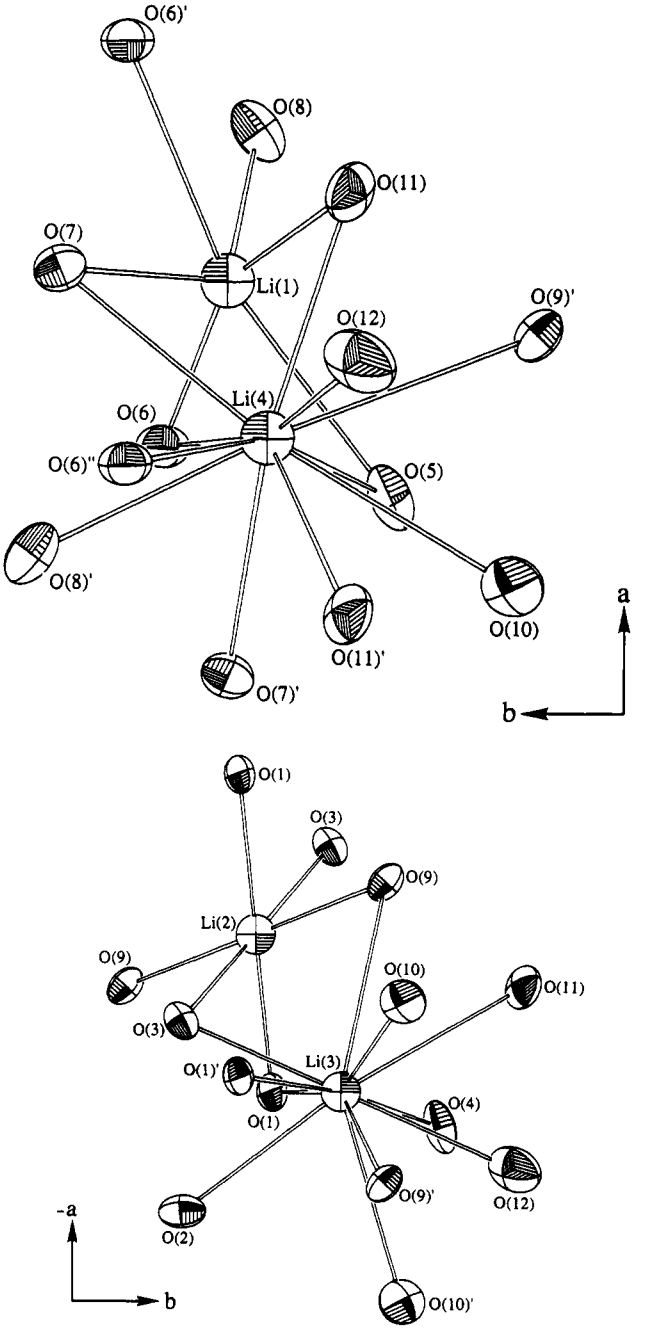

Figure 6. ORTEP drawings of two pairs of double LiO_n polyhedra are viewed along the c axis. (a, top) The $Li(1)O_6$ and $Li(4)O_{11}$ polyhedra share a common plane made of O(5), O(6), O(7), and O(11). (b, bottom) The $Li(2)O_6$ and $Li(3)O_{11}$ polyhedra share O(1), O(3), and O(9), and while the O(4) atom is detached from Li(2) (see text). All the thermal ellipsoids for the oxygen atoms are drawn at a 90% probability.

The doubling of the b axis has created a total of four new lithium atom sites in an asymmetric unit. These four asymmetric lithium sites can be grouped into two pairs. Each pair consists of a cage and a channel lithium atom, i.e., Li(1) and Li(4) vs Li(2) and Li(3), respectively, and is comparable with the asymmetric unit found in the x = 1.72 structure. In the currently studied structure there is subtle difference between the two corresponding cage lithium atoms, Li(1) and Li(2). The former occurs at a general position, while the latter is found at the inversion center and consequently its multiplicity is reduced by a half. This crystallographic rearrangement, governed by the composition of the compound, determines the connectivity of the LiO_n polyhedron that in part describes the

Table V. Selected Interatomic Distances[a] (Å) for LiO_n Polyhedra in $Li_{1.78}Ti_2(PO_4)_3$

$Li(1)O_6$		$Li(2)O_6$	
Li(1)–O(5)	2.894 (10)	Li(2)–O(1)	2.374 (4) × 2
Li(1)–O(6)	1.926 (9)	Li(2)–O(3)	2.196 (3) × 2
Li(1)–O(6)′	2.956 (9)	Li(2)–O(9)	2.225 (3) × 2
Li(1)–O(7)	2.026 (10)		
Li(1)–O(8)	1.986 (10)		
Li(1)–O(11)	1.994 (10)		
$Li(3)O_{11}$		$Li(4)O_{11}$	
Li(3)–O(1)	2.19 (10)	Li(4)–O(5)	2.4 (1)
Li(3)–O(1)′	2.74 (10)	Li(4)–O(6)	2.1 (1)
Li(3)–O(2)	2.85 (10)	Li(4)–O(6)″	2.9 (1)
Li(3)–O(3)	2.49 (10)	Li(4)–O(7)	2.8 (1)
Li(3)–O(4)	2.74 (10)	Li(4)–O(7)′	3.2 (1)
Li(3)–O(9)′	2.43 (10)	Li(4)–O(8)′	2.8 (1)
Li(3)–O(9)	3.14 (10)	Li(4)–O(9)′	3.1 (1)
Li(3)–O(10)	2.10 (10)	Li(4)–O(10)	3.1 (1)
Li(3)–O(10)′	3.14 (10)	Li(4)–O(11)	2.7 (1)
Li(3)–O(11)	3.1 (1)	Li(4)–O(11)′	3.0 (1)
Li(3)–O(12)	2.76 (10)	Li(4)–O(12)	2.0 (1)
Li(1)–Li(4)	2.2 (1)	Li(2)–Li(3)	2.93 (10)

[a] The first longest, nonlisted Li–O distances are 3.29, 3.49, 3.33, and >3.60 Å for Li(1), Li(2), Li(3), and Li(4), respectively. The O–O distances are in the range of 2.45–3.33 Å.

geometry as well as the size of the cage and channel structures.

In Figure 6, two pairs of interconnected lithium polyhedra are viewed along the c axis. The view has been purposely chosen to allow one to distinguish the difference in connectivity of the LiO_n polyhedra. The LiO_n polyhedra are described by the appropriate Li–O distances, as listed in Table V. The coordination number (n) is arbitrarily chosen based upon the cutoff point where the $(Li–O)_{max}$ distance contributes a minimum of 0.01 to the bond valence sum (see footnote, Table V). Coincidently, the polyhedral size (n) of each corresponding lithium oxide polyhedron is the same, i.e., $Li(1)O_6$ and $Li(4)O_{11}$ (Figure 6a) vs $Li(2)O_6$ and $Li(3)O_{11}$ (Figure 6b). The geometries of these two pairs of interconnected LiO_n polyhedra seem very similar at first glance, yet they are somewhat different in connectivity due to the difference in geometries of the $Li(1)O_6$ and $Li(2)O_6$, polyhedra. The geometry of the $Li(1)O_6$ polyhedron is quite irregular, while the $Li(2)O_6$ polyhedron can be described as a slightly distorted octahedron. Because of this difference, the connectivity between LiO_6 and LiO_{11} is also varied. The common face of the fused $Li(1)O_6$ and $Li(4)O_{11}$ polyhedra consists of four oxygen atoms to form a twisted square plane, i.e., O(5), O(6), O(7), and O(11). However, the other fused polyhedral pair, $Li(2)O_6$ and $Li(3)O_{11}$, share a triangular face of the $Li(2)O_6$ octahedron, i.e., O(1), O(3), and O(9). The fourth oxygen atom in the latter case, O(4), which supposedly could be used for the formation of a similar square plane, is not a part of the $Li(2)O_6$ polyhedron. Subsequently, a longer Li–Li separation is observed in Li(2)–Li(3), 2.9 (1) Å, than in Li(1)–Li(4), 2.2 (1) Å. The shorter Li–Li separation is comparable with that found in the previously discussed x = 1.72 phase, i.e., 2.29 (5) Å. Nevertheless, the two polyhedral pairs have similar averaged Li–O distances, i.e., 2.30 Å for Li(1)–O vs 2.27 Å for Li(2)–O and 2.70 Å for Li(3)–O vs 2.73 Å for Li(4)–O. It should be noted that the average size of both polyhedra in the currently studied structure is relatively larger than that found in the structure of the x = 1.72 phase.

Structural Relationship with x = 0.00 (NASICON Structure) and 1.72 ($Sc_2(WO_4)_3$ Type) Phases. Although the projected structure (Figure 4) of this new, structurally characterized compound, $Li_{1.78}Ti_2(PO_4)_3$, looks similar to the previously reported $Li_{2.72}Ti_2(PO_4)_3$ (with a

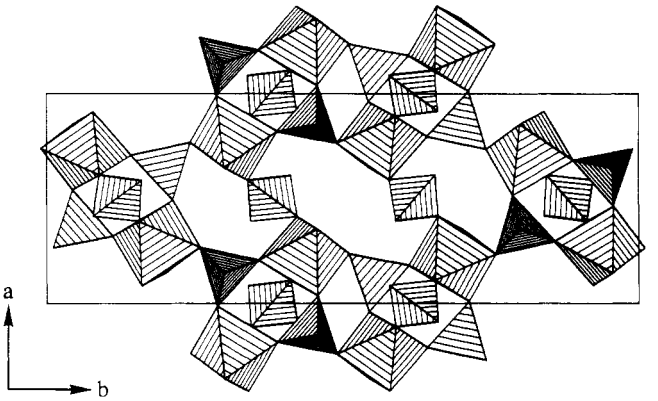

Figure 7. Slab structure built up from $Ti_2(PO_4)_3$ double units and PO_4 tetrahedra shown by a STRUPLO 86 polyhedral plot, viewed along c.

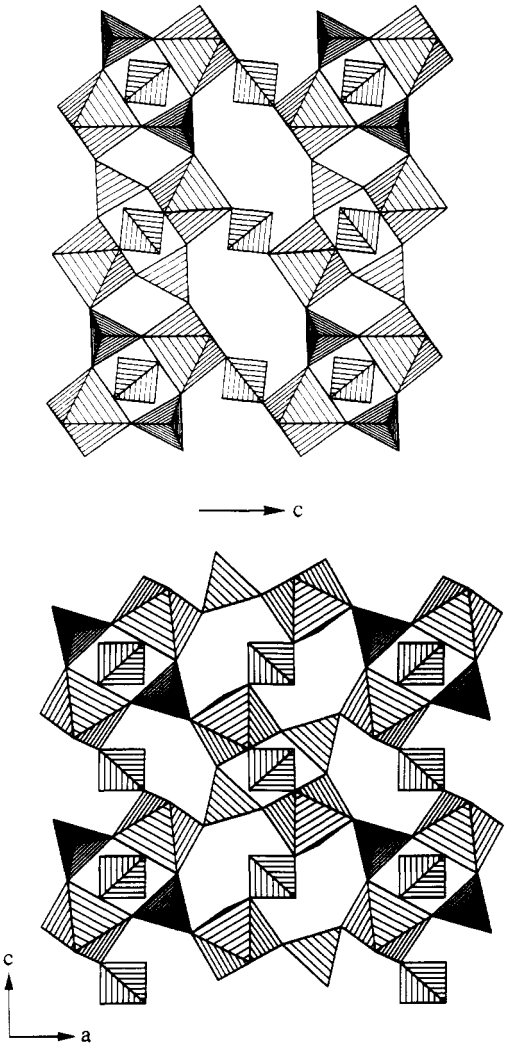

Figure 8. For comparison, the slab structures of (a, top) x = 0.00 phase (NASICON structure) and (b, bottom) $Li_{2.72}Ti_2(PO_4)_3$ are shown.

$Sc_2(WO_4)_3$ type structure[20] and even to NASICON and its related structures, it has an original structure, as stated above. The basic structure dissimilarity in the compounds associated with the NASICON structure is observed in the connectivity of the $M_2(PO_4)_3$ units. In the currently studied structure of $Li_{1.78}Ti_2(PO_4)_3$, the framework consists

(20) Abrahams, S. C.; Bernstein, J. L. *J. Chem. Phys.* **1966**, *45*, 2745.

of double $Ti_2(PO_4)_3$ units that share corner oxygen atoms, as shown in the slab structure in Figure 7. The slab structure is extended along the *ab* plane by interconnecting the double units through b-glide planes perpendicular to the *a* axis at $x = {}^1/_4$ and ${}^3/_4$. The top and bottom slabs are related by a c-glide plane, perpendicular to *b* at $y = {}^1/_4$ and ${}^3/_4$, and these parallel slabs are stacked along the *c* axis. The double units are connected so that two sizes of voids (3O + 3T and 4O + 4T) are found in a single slab plane. These cavities are centered by the cage lithium atoms, Li(1) and Li(2), respectively. Furthermore, the larger size void reflects the large isothermal ellipsoid found in Li(2), e.g. $B(eq) = 5$ (1) Å^2 (Table II).

Slab structures, having a similar perspective as the $x = 0.78$ phase in Figure 7, are shown for the $LiTi_2(PO_4)_3$ (Figure 8a, $x = 0.00$, NASICON structure) and the $Li_{2.72}Ti_2(PO_4)_3$ phases (Figure 8b, $x = 1.72$) for comparison. Obviously, the building blocks consist of PO_4 tetrahedra from adjacent slabs and infinite $[Ti_2(PO_4)_3]_\infty$ chains for the $x = 0.00$ phase, and single $Ti_2(PO_4)_3$ units for the $x = 1.72$ phase. All of these differences are believed to be associated with the composition of lithium and consequently the Ti^{3+}/Ti^{4+} cation distribution. This comparison illustrates the close relationship of NASICON to its structurally related compounds and yet, the apparent differences in the structures are not related by a simple distortion. Last, it is found that the number of large voids (characterized by 4O + 4T) decreases as the concentration of the lithium is increased. It would be interesting to see, then, how the ionic transport properties change as the number of larger voids is diminished. Experiments for the detailed conductivity measurements are planned.

Conclusion

Three solid solution regions in the $Li_{1+x}Ti_2(PO_4)_3$ series are observed, e.g., $0.00 \le x \le 0.50$ (I), $0.50 < x < 1.20$ (II), and $1.20 \le x \le 2.00$ (III). Regions I, II, and III represent the extended solid solutions of the above mentioned $x = 0.00$ (NASICON structure), 0.78 and 1.72 ($Sc_2(WO_4)_3$ type) phases, respectively. X-ray single-crystal structure studies for the $x = 0.78$ phase have shown an original structure that is closely related to the NASICON structure. The solid solution series $Li_{1+x}Ti_2(PO_4)_3$ and the crystal structures of the $x = 0.78$ and 1.72 phases provide an integrated system for the systematic study of the relationship between ionic conductivity and framework structures (including phase transformation, cavity geometry, etc.).

Acknowledgment is made to the National Science Foundation, Solid State Chemistry (SGER, Grant DMR-9012983), and the donors of the Petroleum Research Fund, administered by the American Chemical Society for support of this research. Financial support for the single-crystal X-ray diffractometer by the National Science Foundation is gratefully acknowledged. The authors are indebted to Professor D. Calahan for scanning electron microscopy photographs.

Registry No. $Li_{1-3}Ti_2(PO_4)_3$, 119536-20-8; $Li_{1.78}Ti_2(PO_4)_3$, 140225-42-9; $LiTi_2(PO_4)_3$, 30622-39-0; $Li_{2.72}Ti_2(PO_4)_3$, 119536-22-0.

Supplementary Material Available: Table SI listing anisotropic thermal parameters and Table SII listing refined lattice parameters for polycrystalline $Li_{1+x}Ti_2(PO_4)_3$, $0.00 \le x \le 2.00$ (2 pages); Table SIII, observed and calculated structure factors (11 pages). Ordering information is given on any current masthead page.

Preparation, Solid-State Characterization, and Surface Chemistry of High Surface Area $Ni_xAl_{2-2x}O_{3-2x}$ Mixed Oxides

Guido Busca,* Vincenzo Lorenzelli, and Vicente Sanchez Escribano†

Istituto di Chimica, Facoltà di Ingegneria, Università di Genova P.le Kennedy, I-16129 Genova, Italy

Received October 9, 1991. Revised Manuscript Received January 23, 1992

High surface area $Ni_xAl_{2-2x}O_{3-2x}$ oxides have been prepared ($x = 0$, 0.33, 0.44, 0.5, 0.66, 0.85, 1) by a coprecipitation procedure. Both the precipitates and the calcined materials have been characterized structurally by XRD, FT-IR, and TG-DTG analyses. The precipitates are constituted by boehmite ($x = 0$), by amorphous hydroxy nitrates ($x = 0.33$, 0.44, and 0.5), by a mixed hydroxy-nitrate similar to Takovite ($x = 0.66$), and by the compound $Ni_6Al_2CO_3(OH)_{16}\cdot 4H_2O$, the Ni analogue of hydrotalcite, for $x = 0.85$. The calcined mixed oxides are constituted by the spinel type compounds γ-Al_2O_3 and $NiAl_2O_4$ and their solid solutions for $0 \le x \le 0.5$, while for $x = 0.85$ a rock salt type NiO phase containing Al^{3+} in both tetrahedral and octahedral sites is obtained. For $x = 0.66$ a mixture of the spinel and the rock salt type phase is found. The porosity and the surface structure of the calcined $Ni_xAl_{2-2x}O_{3-x}$ mixed oxides have been investigated by liquid nitrogen adsorption and FT-IR spectroscopy of surface hydroxy group and of adsorbed carbon monoxide and pyridine. The surface composition of these materials, all mesoporous, reflects their bulk structure. Cation vacancy clusters in defective spinels ($x < 0.5$) are responsible for characteristic surface structures. The presence of Al^{3+} in the bulk of rock salt type NiO (sample with $x = 0.85$) results in a deep modification of its acid-base and electronic properties. Precipitation with Na_2CO_3 instead of $(NH_4)_2CO_3$ produces $NiAl_2O_4$, whose surface chemical properties are modified by Na^+ contamination.

Introduction

High surface area homogeneous mixed oxide powders find a number of industrial applications (i.e., in catalysis, adsorption, pigment, sensor, and magnetic technologies[1-4]). To obtain these powders, preparation techniques allowing an intimate mixture of the component ions without high-temperature treatments must be employed. Coprecipitation methods, consisting of the precipitation of mixed hydroxides, hydroxy carbonates or hydroxy nitrates from

† On leave from Departamento de Quimica Inorganica, Facultad de Ciencias Quimicas, Universidad de Salamanca, Spain.

(1) Dadyburior, D. D.; Jewur, S. S.; Ruckenstein, E. *Catal. Rev. Sci. Eng.* **1979**, *19*, 293.
(2) Lew, S.; Jothimurugesan, K.; Flytzani-Stephanopulos, M. *Ind. Chem. Res.* **1989**, *28*, 535.
(3) Shimizu, Y.; Arai, H.; Seiyama, *Sensors Actuators* **1985**, *7*, 11.
(4) Suresh, K.; Kumar, N. R. S.; Patil, K. C. *Adv. Mater.* **1991**, *3*, 148.

0897-4756/92/2804-0595$03.00/0